HPU2 Journal of Sciences:
Natural Sciences and Technology

Journal homepage: https://sj.hpu2.edu.vn

Article type: Research article

An ab initio calculation on the structural, electronic and magnetic properties of Ni-doped $Bi_{0.5}Na_{0.5}TiO_3$

Quoc-Van Duong[a*], Anh-Duong Nguyen[a], Cao-Khang Nguyen[a], Ngoc-Anh Nguyen Thi[a], Chinh-Cuong Nguyen[a], Duc-Dung Dang[b], Tien-Lam Vu[b], Minh-Thu Le[a]

[a]*Hanoi National University of Education, Hanoi, Vietnam*
[b]*Hanoi University of Science and Technology, Hanoi, Vietnam*

Abstract

The first principle calculation was employed to investigate the formation energies and structural, electronic, and magnetic properties of intrinsic and Ni-doped sodium bismuth titanate $Bi_{0.5}Na_{0.5}TiO_3$ (BNT). The obtained formation energies indicate that Ni atoms prefer to dope into Bi-sites in the lattice of BNT while the calculated band structure shows that the doping leads to the emergence of new mid-gap energy states in the bandgaps, reducing the bandgap value of doped materials. The PDOSs reveal that Bi-*6p*, O-*2p* and Ti-*3d* contribute major parts in BNT valence and conduction bands, while the Ni-*3d* and *4s* play the main roles in the formation of new mid-gap states. The spin-resolved density of states, the integrated spin densities and the charge distributions suggest that all doped models exhibit magnetic behavior, mainly due to the interaction of Ni, O and Ti atoms. The study method of this research can be applied to predict new properties of BNT-based materials.

Keywords: BNT, DFT, Ni-doped, electronic structure, magnetic property

1. Introduction

Since discovered by Smolenskii et al [1], [2] in the 1960s, lead-free ferroelectric $Bi_{0.5}Na_{0.5}TiO_3$ (BNT) has become one of the most studied materials worldwide. The ferroelectric behavior of BNT is comparable to that of $Pb(Zr,Ti)O_3$ (PZT) with large remnant polarization of about 40 $\mu C/cm^2$ and large coercive field of around 70 kV/cm [3]. Recently, the discovery of weak ferromagnetic properties at room temperature [4] confirms that BNT can replace PZT in many application areas, especially in the field of smart electronic devices, producing sustainable and environment friendly products and protecting human health [5]. However, the application of BNT is limited by its low magnetization at room

* Corresponding author, E-mail: vandq@hnue.edu.vn

https://doi.org/10.56764/hpu2.jos.2024.3.3.10-19

Received date: 03-5-2024 ; Revised date: 24-7-2024 ; Accepted date: 06-9-2024

temperature [4], [6], approximate 1.0 memu/g, preventing its usage in technology and real-life applications. This limitation has been tried to overcome via different experimental methods: doping with magnetic element likes Fe [7], Co [8], Mg [9]; forming solid solutions or compositing with other magnetic materials such as $CoFe_2O_4$ [10], [11], $BiFeO_3$ [12], $BaNiO_3$, $CaNiO_3$; $MgNiO_3$ or $SrNiO_3$ [13]–[16]; or hybridization of both doping and compositing [12]. The obtained results show that doping with transition elements can clearly improve the magnetic behavior of modified BNT compared to intrinsic material.

However, the origin of the magnetic properties of doped BNT is not clearly explained by both experimental and theoretical views. Thanh et al [17] show that the room temperature ferromagnetic behavior of BNT can be origin from the enhance of oxygen vacancies when Cr cations substituted into Ti-sites in BNT lattice. For Co-doped BNT, while Wang et al [4] prove that the room temperature magnetism of modified BNT arose from Co clusters forming during the crystallization of matter, Dung et al [18], [19] suggest that the origin of this magnetic behavior is the random distribution of Co cations in the lattice of BNT. However, recent studies indicate that the super exchange interactions between transition ions and oxygen vacancy (O^v) such as Fe^{3+}-O^v-Fe^{3+} [7], $Ni^{2+/3+}$-O^v-$Ni^{2+/3+}$ [13] should be considered as the origin of ferromagnetism of Fe- or Ni-modified BNT. In theoretical studies, Dung et al [13]–[16] suggest that the doping of Ni atoms into both Bi-sites and Na-sites in the lattice of BNT clearly influenced the electronic properties of host BNT, inducing the magnetic behavior of materials. On the other hand, Ju et al [20] using VASP to prove that magnetic moment can be induced when transition metal atoms (V, Cr, Mn, Fe or Co) incorporate into Ti-sites instead of Bi- or Na-sites. However, when doped into BNT lattice, Ni atoms can substitute into different position: Bi-sites, Na-sites, Ti-sites, and interstitial sites. The favored doping positions of Ni atoms are not confirmed, so is the origin of the magnetic behavior of Ni-doped BNT.

In this research, a complete theoretical investigation on the origin of magnetic properties of Ni-doped BNT has been performed and analyzed using first principle calculation. Models of possible doping positions of Ni atoms into BNT lattice have been built and investigated to carry out the favorited doping sites, confirming the origin of magnetism of Ni-doped BNT. The method used in this research can be applied to the other doped BNT materials, concluding the causes of the improvement of magnetic properties of doped BNT.

2. Computational methods

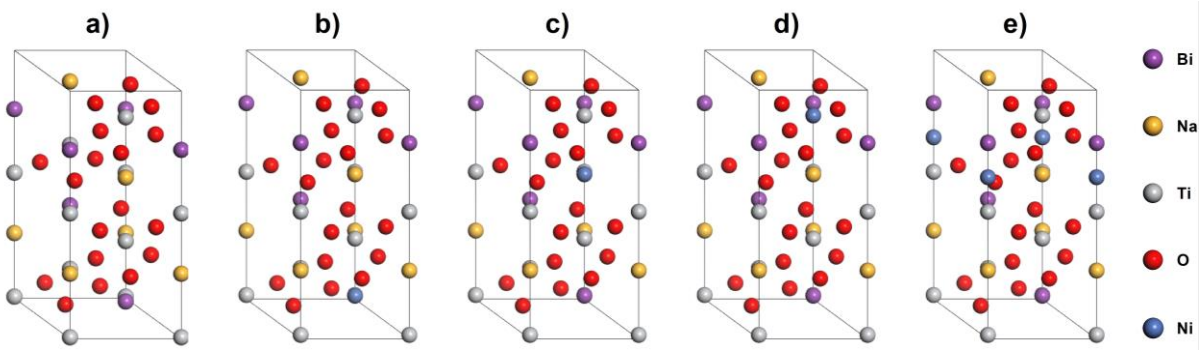

Figure 1. The models of **a)** intrinsic and Ni-doped BNT at **b)** Bi-sites, **c)** Na-sites, **d)** Ti-sites and **e)** interstitial sites.

In this research, a unit cell of intrinsic BNT containing 3 Bi atoms, 3 Na atoms, 6 Ti atoms and 18 O atoms (labelled as BNT, as shown in Figure 1a) was used to study physical properties of material. To investigate the effects of Ni doping on the physical properties of BNT, 4 Ni-modified models were created. Three models of substitutional N-doped supercells were constructed and labelled as B(Ni)NT, BN(Ni)NT and BNT(Ni) for the case of Ni atoms doped into Bi-sites, Na-sites and Ti-sites, respectively; the interstitial Ni-doping model (labelled as BNT+Ni) was constructed by embedding one Ni atom into the interspace of BNT; as shown in Figure 1b-e.

The Cambridge Serial Total Energy (CASTEP) [21], [22], a DFT-based calculation package, was used to investigate the structural, electronic and magnetic properties of intrinsic and Ni-doped BNT materials. The exchange-correlation interactions were described using the Generalized Gradient Approximation (GGA), parameterized with Perdew-Burke-Erzernhof functional [23], [24]. The ultrasoft pseudopotential introduced by Vanderbilt [25] was used to describe the interactions between the core and valence electron: $6s^2 6p^3$ for Bi, $3s^1$ for Na, $3d^2 4s^2$ for Ti, $2s^2 2p^4$ for O and $3d^2 4s^2$ for Ni. The k-points grid, based on Monkhorst-Pack scheme [26], used to calculate in the Brillouin zone was set by 5×5×2 for all models. A cutoff energy of 410 eV has been used for band structure calculation. The calculation processes converge when the change in total energy reaches 5×10^{-6} eV/atom; and the corresponding tolerances for force, stress and displacement were 0.01 eV/Å, 0.02 GPa and 0.005 Å, respectively.

3. Results and discussion

3.1. Formation energies

In general, a more stable and formable model has negative and large magnitude formation energy whereas the positive values indicate that the materials are synthesizable but nonstable. The formation energy ΔEmod of defective BNT models can be calculated as follows [27]:

$$\Delta E_{mod} = E_{tot}\,(\text{models}) - E_{tot}\,(\text{pure}) - m\mu_{\text{Ni}} + n\mu_{\text{Bi}} + p\mu_{\text{Na}} + q\mu_{\text{Ti}}$$

E_{tot} (models) and E_{tot} (pure) are the total energies of Ni-doped and intrinsic BNT models; μ_{Ni}, μ_{Bi}, μ_{Na} and μ_{Ti} represent the chemical potentials of the Ni, Bi, Na and Ti atoms, respectively; m, n, p and q are the numbers of doped Ni atoms and removed Bi, Na and Ti atoms in the models, listed in Table 1.

Table 1. Values of doped Ni atoms (m), removed Bi atoms (n), removed Na atoms (p) and removed Ti atoms (q) for intrinsic and defective BNT models.

Models	BNT	B(Ni)NT	BN(Ni)T	BNT(Ni)	BNT+Ni
m	0	1	1	1	1
n	0	1	0	0	0
p	0	0	1	0	0
q	0	0	0	1	0

The formation energies of defective BNT models were calculated and listed in Table 2. It is known that a smaller formation energy indicates a more stable material, while a higher formation energy suggests that the sample is more difficult to form. It can be seen that BNT(Ni) model has the highest formation energy while B(Ni)NT model has the lowest one; the formation energies of both BN(Ni)T and BNT+Ni models are similar, significantly smaller than that of BNT(Ni) but larger than B(Ni)NT's. The results show that when incorporated into BNT lattice, Ni atoms prefer to replace into Bi-sites rather than the remains. The formation energies of BN(Ni)T and BNT+Ni suggest that the Na-sites or interstitial sites can be taken by Ni atoms at higher doping concentration.

Table 2. Formation energies of Ni-doped BNT models.

BNT	B(Ni)NT	BN(Ni)T	BNT(Ni)	BNT+Ni
Formation Energy (eV)	3.0818	4.1299	8.0630	4.0554

3.2. Structural properties

Table 3. Lattice constants of intrinsic and Ni-doped BNT models.

Models	a = b (Å)	c (Å)	Total Energy (eV)
BNT	5.4939	13.8345	-21882.4689
B(Ni)NT	5.3905	13.8668	-23082.6532
BN(Ni)T	5.4662	13.8705	-21928.4755
BNT(Ni)	5.4659	13.7139	-21625.6576
BNT+Ni	5.5393	14.2491	-23232.7853

Table 3 shows the optimized lattice constants of unit cells of intrinsic and Ni-doped BNT models calculated using CASTEP; the trend of changes in lattice constants and total energies of models was displayed in Figure 2. The achieved lattice constants of BNT models are $a = b = 5.4939$ Å and $c = 13.8345$ Å, in good agreement with calculations and experiments [28], [29] and other theoretical studies [14]. Figure 2a shows that the doping of Ni atoms as a substitution decrease the *a* and *b* values of BNT unit cell, despites of doping sites. This is the results of smaller ionic radius of Ni (0.69 Å) compared to that of Bi (0.76 Å), Na (1.18 Å) or Ti (0.74 Å) [30]. For the interstitial doping, the incorporation of Ni atoms into the interspace of BNT lattice leads to an expansion of unit cells, resulting in larger lattice constant of 5.5393 and 14.2491 Å.

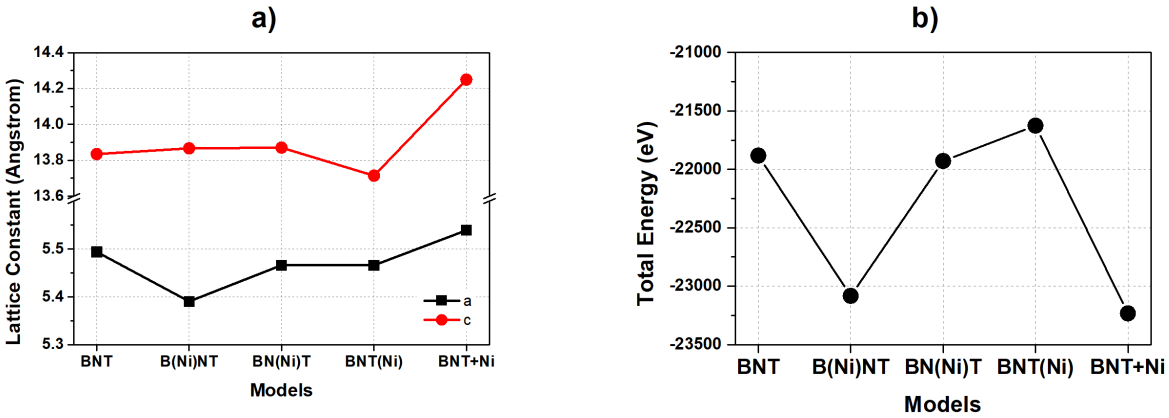

Figure 2. a) Lattice constants and **b)** total of intrinsic and defective BNT mosdels.

Figure 2b shows that B(Ni)NT and BNT+Ni have the lowest calculated total energies, while BNT(Ni) has the highest total energy per unit cell. The results indicate that both B(Ni)NT and BNT+Ni are stable models, and BNT(Ni) is the least stable one, suggesting that when Ni atoms are doped into BNT, B(Ni)NT and BNT+Ni are more formable than BN(Ni)T and BNT(Ni). By comparing these results with the formation energies shown in Table 1, it can be predicted that Ni atoms tend to substitute into Bi-sites or interstitial sites when doped into BNT lattice at low concentration and into both Bi-sites and interstitial-sites at high concentrations.

3.3. Electronic structures

Figure 3 illustrates the calculated band structures and partial density of states of intrinsic and Ni-modified BNT models. Figure 3a shows that BNT is a direct bandgap material with bandgap value of 2.86 eV, the highest energy states in the valence band and the lowest energy state in the conduction

band both occurs at the center point gamma G of Brillouin zone. It can be seen that the Fermi level in BNT is located just on the top of valence bands, suggesting that the material behaves as a *p*-type semiconductor. Figure 3b-e suggest that the incorporation of Ni atoms into the lattice of BNT creates new mid-gap states in the band gap of host material, leading to a decrease of bandgap and shifting the absorption edge of BNT to the longer wavelength zone. The doping of Ni atoms into the BNT lattice also shifted the Fermi levels to the top of valence bands in B(Ni)NT and BNT(Ni) models, opposition with the case of BN(Ni)T and BNT+Ni, whereas the Fermi level located just below the conduction bands. The location of Fermi levels suggest that B(Ni)NT and BNT(Ni) behave as *p*-type semiconductors, while BN(Ni)T and BNT+Ni are *n*-type semiconductors, consistent with Linh et al **[**31**]**. It can be observed that the Fermi level is at the top of valence band for BNT, BNT(Ni) and BNT+Ni but it is located in the mid-gap levels for B(Ni)NT and BN(Ni)T; originating from the shifting of Fermi level due to the incorporate of Ni atoms into doping sites. In general, all the doped Ni atoms creates new mid-gap levels in the bandgap of intrinsic BNT. However, if doping into Bi/Na sites gives additional electron to the material, shifting the Fermi level to the bottom of conduction band, then the incorporate of Ni atoms into Ti-sites or interstitial sites creates more holes in the system and pushing the Fermi level to the top of conduction band. The shift of Fermi levels depends on the number and effective masses of free charge carriers and temperature of materials; resulting in the different positions of Fermi levels as seen on Figure 3.

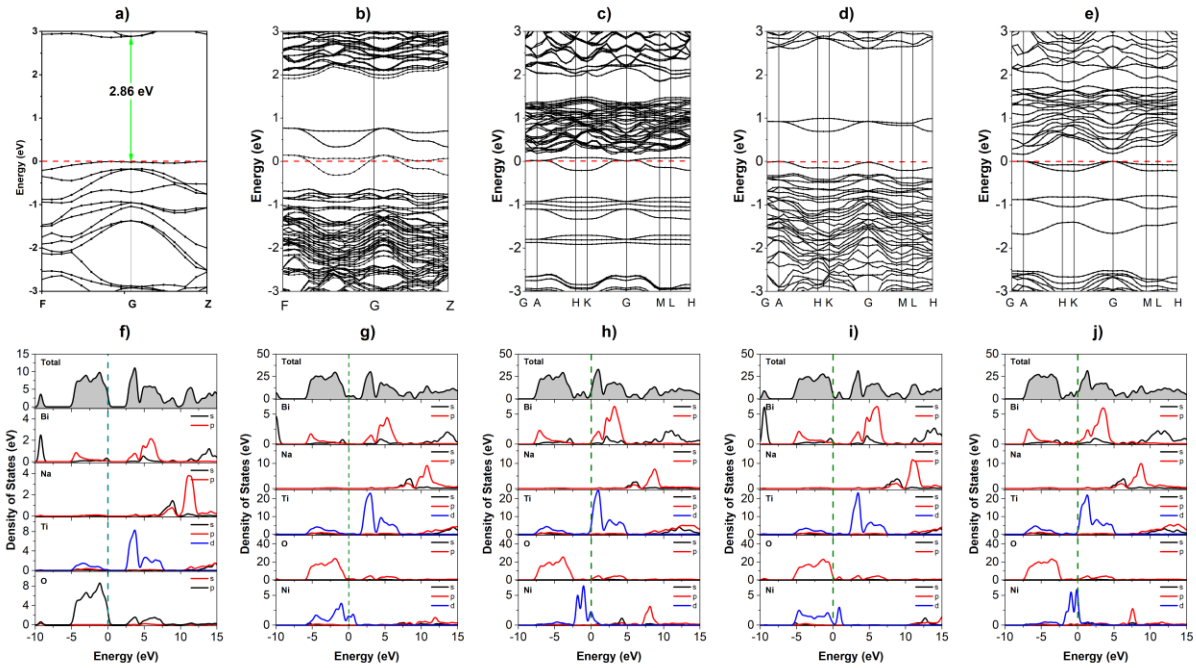

Figure 3. Band structures of **a)** BNT, **b)** B(Ni)NT, **c)** BN(Ni)T, **d)** BNT(Ni) and **e)** BNT+Ni; Partial density of states of **f)** BNT, **g)** B(Ni)NT, **h)** BN(Ni)T, **i)**BNT(Ni) and **j)** BNT+Ni. The Fermi level is set to 0 eV.

The calculated partial densities of states (PDOSs) of intrinsic and modified BNT models are shown in Figure 3f-j. Figure 3f confirms the domination of Bi-*6p*, Ti-*3d* and O-*2p* electrons in the formation of valence and conduction bands of BNT, consistent with previous calculations [13]–[16]. For doped BNT models, it can be seen that the new mid-gap energy levels are caused by the hybridization of Ni-*3d* electrons with *s* and *p* electrons of Bi, Ti and O in the unit cells of BNT, reducing the bandgap value of BNT.

3.4. Magnetic Properties

To study the magnetic properties of Ni-doped BNT, the spin-resolved density of states of all models were calculated and displayed in Figure 4; the majority (spin-up) and minority (spin-down) states are represented by red and blue lines, respectively. The green lines at the bottom of each graph indicate the corresponding calculated spin density of states of each model.

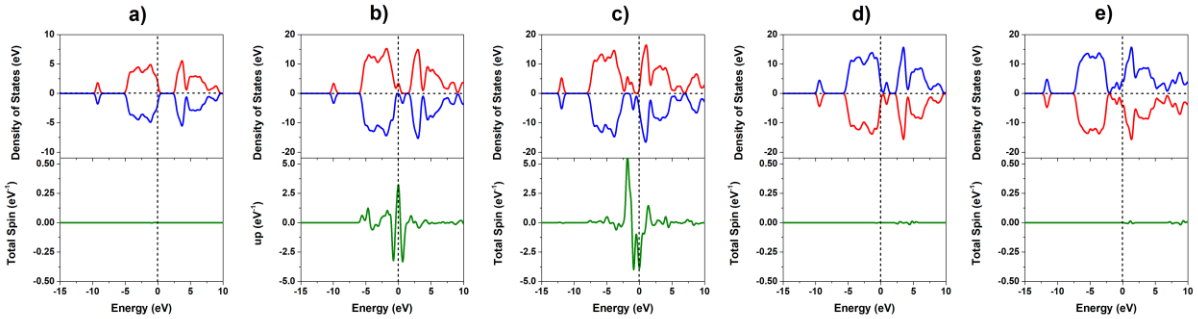

Figure 4. Resolved density of states and spin density of states of **a)** BNT, **b)** B(Ni)NT, **c)** BN(Ni)T, **d)** BNT(Ni) and **e)** BNT+Ni models. The red lines represent for spin up electrons, the blue lines represent for spin down electrons. The Fermi level is set to 0 eV.

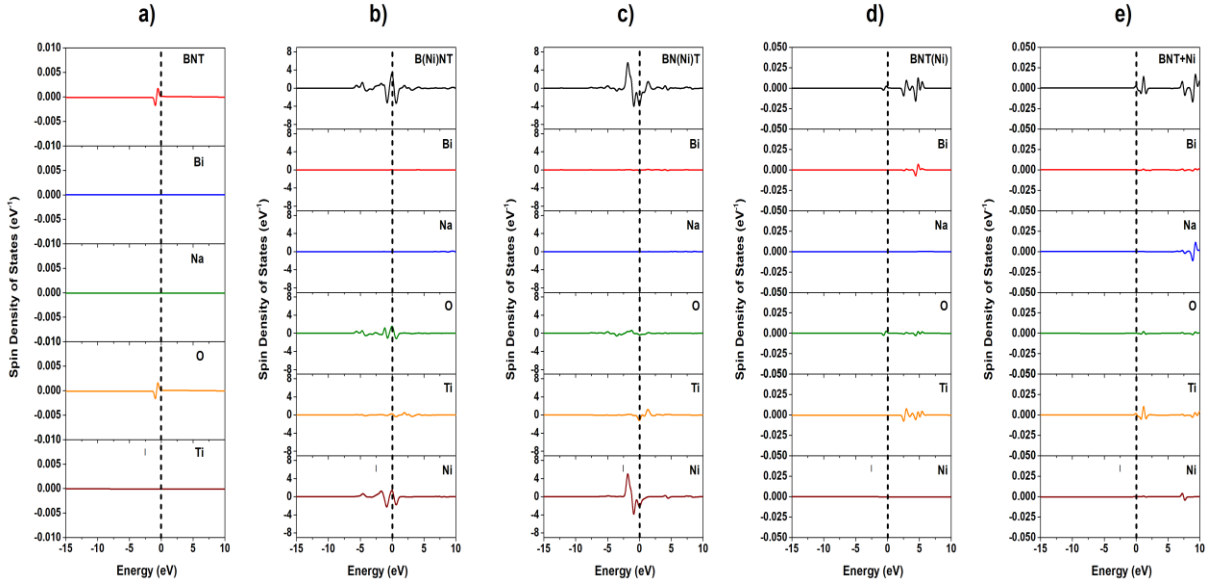

Figure 5. Total spin density of states and contribution of elements in **a)** BNT, **b)** B(Ni)NT, **c)** BN(Ni)T, **d)** BNT(Ni) and **e)** BNT+Ni models. The Fermi level is set to 0 eV.

The symmetric shape of majority and minority spin states in the BNT model, shown in Figure 4a, indicates that BNT is a non-magnetic material, consistent with experimental results and previous calculations. The clearly asymmetric shape of the spin-up and spin-down spin states of B(Ni)NT and BN(Ni)T (Figure 4b-c) in the range of about -3 eV to 3 eV suggests that B(Ni)NT and BN(Ni)T are strong magnetic materials, which is consistent with their calculated total spin densities in Figure 5b-c, in good agreement with Dung et al [13]. However, for BNT(Ni) and BNT+Ni models, as shown in Figure 4d-e, a small asymmetric of the spin-resolved density of states can be observed around +5 eV and +10 eV, suggesting that these models exhibit weak magnetic behaviors. The obtained results suggest that Ni dopants play an important role in magnetic properties of modified materials, especially in Bi-sites and Na-sites doping.

For further investigations, the total spin density of states of intrinsic and Ni-doped BNT models and the contribution of elements were calculated and illustrated in Figure 5; the integrated spin densities and maximum spin per atom are listed in Table 4. Figure 5a reveals that BNT may exhibit weak magnetic behavior, originating from O atoms without the contributions of Bi, Na or Ti atoms. Figures 5b and 5c show that the strong magnetic behaviors of B(Ni)NT and BN(Ni)T models are dominated by Ni-O and Ti-O interactions, while Figure 5d-e suggest that the weak magnetic behaviors of BNT(Ni) and BNT+Ni arises primarily from doped Ni atoms, consistent with the maximum spin per atom of the models listed in Table 4, and charged distribution shown in Figure 6. The integrated spin density (ISD) and integrated |spin density| (I|SD|) of the models in Table 4 also show that BNT, BNT(Ni) and BNT+Ni exhibit weak ferrimagnetic behaviors while B(Ni)NT and BN(Ni)T are strong ferromagnetic materials [32].

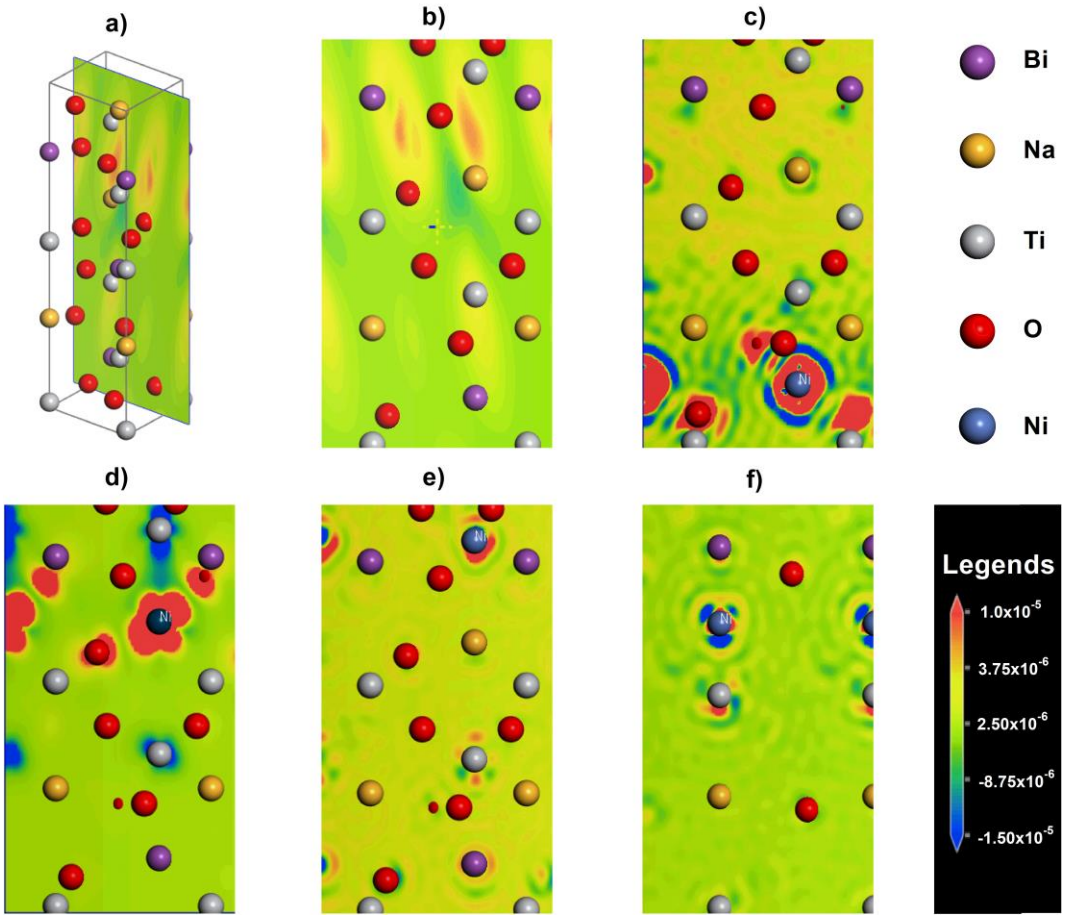

Figure 6. Calculated charged distribution of BNT models: **a)** slice for charge, contour plot for **b)** BNT, **c)** B(Ni)NT, **d)** BN(Ni)T, **e)** BNT(Ni) and **f)** BNT+Ni.

The calculated charge distribution of all BNT-based models within a selected slice are shown in Figure 6; the selected slice for contour is shown in Figure 6a. It is clear that the increase of spin densities is significant around Ni atom for all models, as shown in Figure 6b-f, and around O atoms in B(Ni)NT and BN(Ni)T models, as shown in Figure 6c-d; in good agreement with projected spin densities of states in Figure 5. In another word, the doping of Ni atoms into BNT lattice in both substitute and interstitial position produces magnetic moments for materials, the strongest magnetic behavior can be obtained for Bi-site and Na-sites substitution.

Table 4. The integrated spin density (ISD), integrated |spin density| (I|SD|), magnetic behavior and maximum spin per atoms in pure and defective BNT models.

Models	**ISD** $\left(\frac{\hbar}{2}\right)$	**I|SD|** $\left(\frac{\hbar}{2}\right)$	**Magnetic Behavior**	**Maximum spin per atom** $\left(\frac{\hbar}{2}\right)$				
				Bi	**Na**	**O**	**Ti**	**Ni**
BNT	-1.7×10^{-14}	7.4×10^{-4}	Ferrimagnetic	0	0	0	0	
B(Ni)NT	0.99	1.06	Ferromagnetic	0	0	**0.04**	0	**0.71**
BN(Ni)T	1.00	1.81	Ferromagnetic	0	0	**0.04**	**-0.16**	**1.14**
BNT(Ni)	-8.1×10^{-4}	4.7×10^{-3}	Ferrimagnetic	0	0	0	0	0
BNT+Ni	-3.5×10^{-4}	9.3×10^{-3}	Ferrimagnetic	0	0	0	0	0

4. Conclusion

In this study, intrinsic, substitutional and interstitial Ni-doped BNT models have been modelled and investigated. The calculated formation energy suggest that the Ni atoms prefer to dope into BNT lattice at Bi-sites rather than Na- and interstitial- sites, and the Ti-sites doping is the most difficult to achieved. The electronic structure results show that intrinsic BNT is a *p*-type and direct bandgap semiconductor with bandgap energy of 2.86 eV; the band structures of BNT are dominated by the interaction of Bi-*6p*, Ti-*3d* and O-*2p* electrons. The incorporation of Ni atoms into BNT lattice creates new mid-gap energy states in the bandgap of BNT, reducing bandgap energies of doped models. The total spin density of states, the maximum spin per atom and the charge distributions of models show that the incorporation of Ni into the BNT lattice produces stronger magnetic behavior for all doped models.

Acknowledgement

This research is funded by Ministry of Education and Training of Vietnam (MOET), under grant number B2023-SPH-18.

References

[1] G. A. Smolenskii and A. I. Agranovskaya, "Dielectric polarization of a number of complex compounds," *Sov. phys., Solid state*, vol. 1, no. 10, pp. 1429–1437, 1960.

[2] G. A. Smolenskii and A. I. Agranovskaya, "New ferroelectrics of complex composition. IV," *Sov. phys., Solid state*, vol. 2, pp. 2651–2654, Jan. 1961.

[3] S. -E. Park, S. -J. Chung, and I. -T. Kim, "Ferroic phase transitions in $(Na_{1/2}Bi_{1/2})TiO_3$ crystals," *J. Am. Ceram. Soc.*, vol. 79, no. 5, pp. 1290–1296, May 1996, doi: 10.1111/j.1151-2916.1996.tb08586.x.

[4] Y. Wang *et al.*, "Room-temperature ferromagnetism of Co-doped $Na_{0.5}Bi_{0.5}TiO_3$: Diluted magnetic ferroelectrics," *J. Alloys Compd.*, vol. 475, no. 1–2, pp. L25–L30, May 2009, doi: 10.1016/j.jallcom.2008.07.073.

[5] W. Zhu *et al.*, "A review: $(Bi,Na)TiO_3$ (BNT)-based energy storage ceramics," *J. Mater.*, vol. 10, no. 1, pp. 86–123, Jan. 2024, doi: 10.1016/j.jmat.2023.05.002.

[6] Y. Wang *et al.*, "Room temperature ferromagnetism in Fe-doped $Na_{0.5}Bi_{0.5}TiO_3$ crystals," *Mater. Sci.-Pol.*, vol. 27, no. 2, pp. 471–476, Jan. 2009.

[7] D. D. Dung *et al.*, "Tunable magnetism of $Na_{0.5}Bi_{0.5}TiO_3$ materials via Fe defects," *J. Supercond. Nov. Magn.*, vol. 32, no. 10, pp. 3011–3018, Jun. 2019, doi: 10.1007/s10948-019-05163-z.

[8] P. Bhupaijit *et al.*, "Effect of Co^{2+} substitution in B-sites of the perovskite system on the phase formation, microstructure, electrical and magnetic properties of $Bi_{0.5}(Na_{0.68}K_{0.22}Li_{0.10})_{0.5}TiO_3$ ceramics," *Int. J. Miner. Metall. Mater.*, vol. 29, no. 9, pp. 1798–1808, Jul. 2022, doi: 10.1007/s12613-021-2345-8.

[9] Y. Qiao *et al.*, "Ba and Mg co-doping to suppress high-temperature dielectric loss in lead-free $Na_{0.5}Bi_{0.5}TiO_3$-based systems," *J. Eur. Ceram. Soc.*, vol. 40, no. 3, pp. 720–727, Mar. 2020, doi: 10.1016/j.jeurceramsoc.2019.11.029.

[10] M. Cernea *et al.*, "Magnetoelectric properties of $CoFe_2O_4$/BNT–BT0.08 biphasic nanocomposites, with 0–3 connectivity, prepared by sol-gel method," *J. Alloys Compd.*, vol. 952, pp. 170041–170041, Aug. 2023, doi: 10.1016/j.jallcom.2023.170041.

[11] M. Cernea *et al.*, "Composite BNT-BT0.08/$CoFe_2O_4$ with core-shell nanostructure for piezoelectric and ferromagnetic applications," *Mater. Sci. Eng. B: Solid-State Mater. Adv. Technol.*, vol. 240, pp. 7–15, Jan. 2019, doi: 10.1016/j.mseb.2019.01.001.

[12] M. Cernea *et al.*, "$BiFeO_3$ doped-BNT-BT0.08 piezoelectric and magnetic nanowires, derived from sol–gel precursor," *J. Nanoparticle Res.*, vol. 16, no. 2, p. 2231, Jan. 2014, doi: 10.1007/s11051-013-2231-z.

[13] D. D. Dung *et al.*, "Synthesis and characterization of $(1-x)Bi_{1/2}Na_{1/2}TiO_3 + xSrNiO_{3-\delta}$ solid solution system," *J. Electron. Mater.*, vol. 51, no. 6, pp. 2716–2731, Mar. 2022, doi: 10.1007/s11664-022-09534-6.

[14] D. D. Dung *et al.*, "Structural, optical, and magnetic properties of a new complex $(1-x)Bi_{1/2}Na_{1/2}TiO_3 + xMgNiO_{3-\delta}$ solid solution system," *Appl. Phys. A: Mater. Sci. Process.*, vol. 128, no. 2, p. 129, Jan. 2022, doi: 10.1007/s00339-021-05255-5.

[15] D. D. Dung *et al.*, "Magnetic properties of a $(1-x)Bi_{0.5}Na_{0.5}TiO_3 + xCaNiO_{3-\delta}$ solid solution system prepared by sol–gel technique," *J. Electron. Mater.*, vol. 51, no. 5, pp. 1905–1921, Feb. 2022, doi: 10.1007/s11664-022-09457-2.

[16] D. D. Dung *et al.*, "Magnetic properties of new $(1-x)Bi_{1/2}Na_{1/2}TiO_3 + xBaNiO_{3-\delta}$ solid solution materials," *Appl. Phys. A: Mater. Sci. Process.*, vol. 128, no. 2, p. 168, Feb. 2022, doi: 10.1007/s00339-022-05281-x.

[17] L. T. H. Thanh *et al.*, "Origin of room temperature ferromagnetism in Cr-doped lead-free ferroelectric $Bi_{0.5}Na_{0.5}TiO_3$ materials," *J. Electron. Mater.*, vol. 46, no. 6, pp. 3367–3372, Jan. 2017, doi: 10.1007/s11664-016-5248-0.

[18] D. D. Dung *et al.*, "Role of Co dopants on the structural, optical and magnetic properties of lead-free ferroelectric $Na_{0.5}Bi_{0.5}TiO_3$ materials," *J. Sci.: Adv. Mater. Devices*, vol. 4, no. 4, pp. 584–590, Dec. 2019, doi: 10.1016/j.jsamd.2019.08.007.

[19] D. D. Dung *et al.*, "Experimental and theoretical studies on the room-temperature ferromagnetism in new $(1-x)Bi_{1/2}Na_{1/2}TiO_3 + xCoTiO_3$ solid solution materials," *Vacuum*, vol. 179, Sep. 2020, Art. no. 109551, doi: 10.1016/j.vacuum.2020.109551.

[20] L. Ju, T. -S. Xu, Y. -J. Zhang, and L. Sun, "First-principles study of magnetism in transition metal doped $Na_{0.5}Bi_{0.5}TiO_3$ system," *Chin. J. Chem. Phys.*, vol. 29, no. 4, pp. 462–466, Aug. 2016, doi: 10.1063/1674-0068/29/cjcp1602023.

[21] S. J. Clark *et al.*, "First principles methods using CASTEP," *Z. fur Krist. -Cryst. Mater.*, vol. 220, no. 5–6, pp. 567–570, Jan. 2005, doi: 10.1524/zkri.220.5.567.65075.

[22] M. D. Segall *et al.*, "First-principles simulation: Ideas, illustrations and the CASTEP code," *J. Phys. Condens. Matter.*, vol. 14, no. 11, pp. 2717–2744, Mar. 2002, doi: 10.1088/0953-8984/14/11/301.

[23] J. P. Perdew, K. Burke, and M. Ernzerhof, "Generalized gradient approximation made simple," *Phys. Rev. Lett.*, vol. 77, no. 18, pp. 3865–3868, Oct. 1996, doi: 10.1103/physrevlett.77.3865.

[24] J. P. Perdew *et al.*, "Atoms, molecules, solids, and surfaces: Applications of the generalized gradient approximation for exchange and correlation," *Phys. Rev. B*, vol. 46, no. 11, pp. 6671–6687, Sep. 1992, doi: 10.1103/physrevb.46.6671.

[25] D. Vanderbilt, "Soft self-consistent pseudopotentials in a generalized eigenvalue formalism," *Phys. Rev. B*, vol. 41, no. 11, pp. 7892–7895, Apr. 1990, doi: 10.1103/physrevb.41.7892.

[26] H. J. Monkhorst and J. D. Pack, "Special points for Brillouin-zone integrations," *Phys. Rev. B*, vol. 13, no. 12, pp. 5188–5192, Jun. 1976, doi: 10.1103/physrevb.13.5188.

[27] D. Q. Van, L. M. Thu, and N. M. Thuy, "V-doped TiO_2 anatase: Calculation and experiment," *Journal of Science of HNUE: Math and Phys. Sci.*, vol. 62, no. 8, pp. 127–134, Sep. 2017.

[28] H. Lü, S. Wang, and X. Wang, "The electronic properties and lattice dynamics of $(Na_{0.5}Bi_{0.5})TiO_3$: From cubic to tetragonal and rhombohedral phases," *J. Appl. Phys.*, vol. 115, no. 12, Mar. 2014, Art. no. 124107, doi: 10.1063/1.4869733.

[29] G. O. Jones and P. A. Thomas, "Investigation of the structure and phase transitions in the novel A-site substituted distorted perovskite compound $Na_{0.5}Bi_{0.5}TiO_3$," *Acta Crystallogr. B: Struct. Sci. Cryst. Eng. Mater.*, vol. 58, no. 2, pp. 168–178, Mar. 2002, doi: 10.1107/s0108768101020845.

[30] R. D. Shannon, "Revised effective ionic radii and systematic studies of interatomic distances in halides and chalcogenides," *Acta Crystallogr. A: Found. Adv.*, vol. 32, no. 5, pp. 751–767, Sep. 1976, doi: 10.1107/s0567739476001551.

[31] N. H. Linh, N. H. Tuan, D. D. Dung, P. Q. Bao, B. T. Cong, and L. T. H. Thanh, "Alkali metal-substituted bismuth-based perovskite compounds: A DFT study," *J. Sci.: Adv. Mater. Devices*, vol. 4, no. 3, pp. 492–498, Sep. 2019, doi: 10.1016/j.jsamd.2019.06.005.

[32] J. Goldsby, S. Raj, S. Guruswamy, and D. D. Azbill, "First-principle and experimental study of a gadolinium-praseodymium-cobalt pseudobinary intermetallic compound," *J. Mater.*, vol. 2015, Jun. 2015, Art. no. 753612, doi: 10.1155/2015/753612.